

Activation Layer Stabilization of High Polarization Photocathodes in Sub-Optimal RF Gun Environments

Gregory Mulhollan: Principal Investigator

SLAC National Accelerator Laboratory, Menlo Park, CA 94025
Saxet Surface Science, 3913 Todd Lane, Suite 303, Austin, TX 78744

Abstract. We have developed an activation procedure by which the reactivity to CO₂, a principal cause of yield decay for GaAs photocathodes, is greatly reduced. The use of a second alkali in the activation process is responsible for the increased immunity of the activated surface. The best immunity was obtained by using a combination of Cs and Li without any loss in near bandgap yield. Optimally activated photocathodes have nearly equal quantities of both alkalis.



**Activation Layer Stabilization of High Polarization Photocathodes
in Sub-Optimal RF Gun Environments**

Saxet Surface Science, 3913 Todd Lane, Suite 303, Austin, TX 78744

Principal Investigator: Gregory Mulhollan

III. Phase I results

A. Summary

We have developed an activation procedure by which the reactivity to CO₂, a principal cause of yield decay for GaAs photocathodes, is greatly reduced. The use of a second alkali in the activation process is responsible for the increased immunity of the activated surface. The best immunity was obtained by using a combination of Cs and Li without any loss in near bandgap yield. Optimally activated photocathodes have nearly equal quantities of both alkalis.

B. Modification of test system

The Saxet cathode test system was modified by the addition of the multi-alkali dispenser flange shown below in figures 6 and 7. The flange was designed to hold Cs, Rb, K, Na and Li SAES channel sources. Two Cs assemblies were included to insure that the Cs sources would not deplete before the completion of the experiments. Stainless steel flags attached to nickel risers were positioned between different dispenser types to minimize cross contamination. A second leak valve was added to the chamber to allow dosing with carbon dioxide (99.998% pure research grade). The multi-alkali source flange after installation into the test chamber and bakeout is shown in figure 8. Following the bakeout, each alkali source drive current was increased until photocurrent was obtained from a bulk GaAs photocathode. The starting current used was that for Cs. The operating currents obtained in this way were subsequently re-examined with fresh photocathode material resulting overall in the lowering of the operating point by one to two tenths of an ampere. The currents used for the duration of these test were:

Cs-3.6 A, Rb- 4.6 A, K-4.6 A, Na-5.0 A and Li-6.4 A.

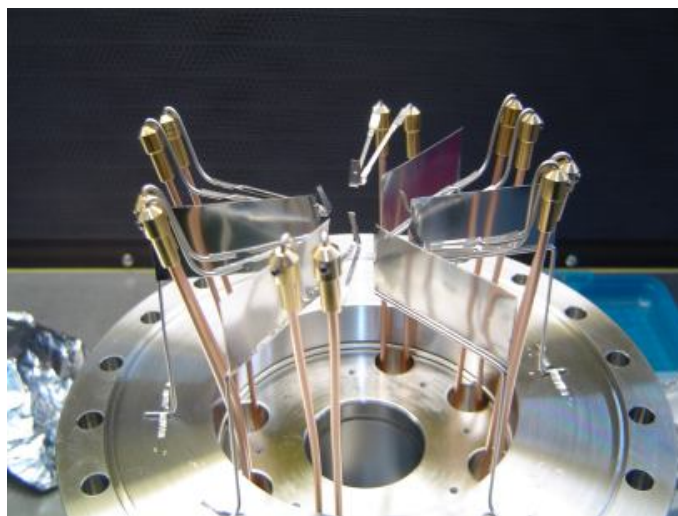


Figure 6. Side view of alkali source flange. Flags were inserted between dispensers of different alkalis to minimize cross-contamination.

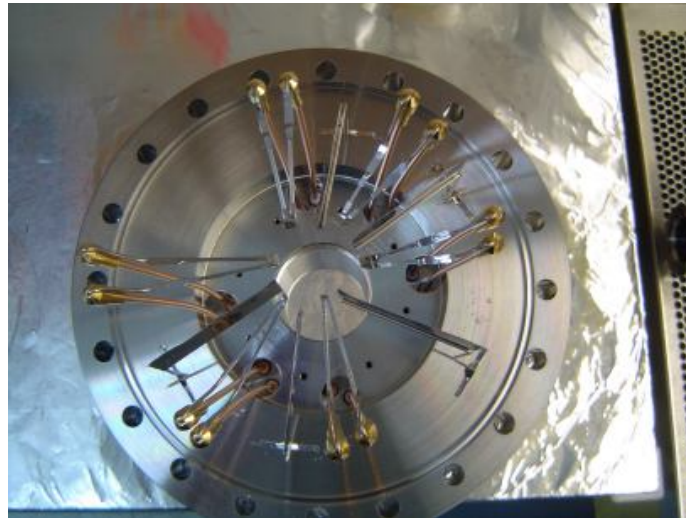


Figure 7. Top view of alkali source flange. The sources are angled toward the location of the sample at chamber center. Each feedthrough has two series-joined dispensers attached to it. The light admitting viewport is mounted on the bottom of the 6" to 2-3/4" adaptor flange.

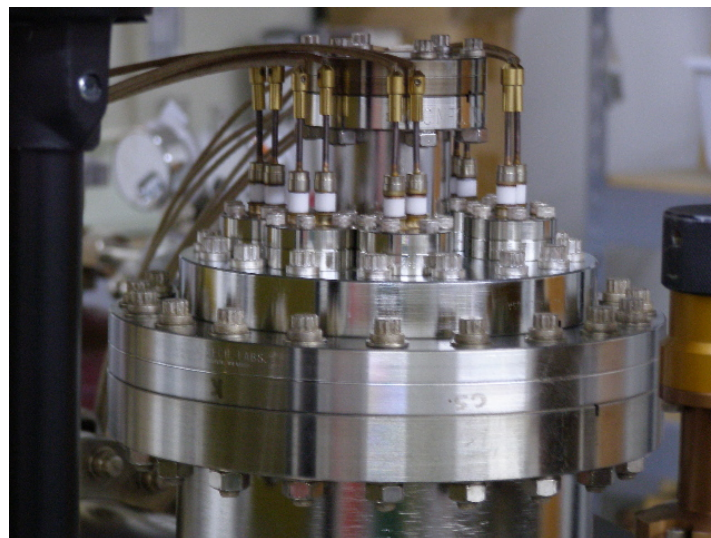


Figure 8. Alkali source flange on chamber after bakeout. High temperature wire was used for the connections so that the sources could be outgassed during the bake.

C. Two-alkali recipes and sensitivity of two-alkali activated cathodes

Initial tests consisted of performing full activations with all alkali metals singly to fully outgas the sources and to establish proper operating currents. Bulk GaAs was used except where noted. Activations were started with a white light source, then finished with a HeNe laser. Photocurrent was kept low at all times by use of neutral density filters to minimize electron beam induced desorption. Lifetime measurements were acquired under computer control. Between data points,

the bias was electronically disconnected and the light source shuttered to inhibit dark current. A comparison of Cs only and Na only activated bulk GaAs is shown below in figure 9. Rb activated bulk GaAs exhibited only marginally worse photoyield than the Cs activated surface. Conversely, the photoyield from the Na activated surface serves to illustrate the disparity in the affinities when the lighter alkalis were used for activation. In keeping with the hypothesis of section I.E., the first dual alkali activations were performed by increasing the second alkali source current to the operating value when the photocathode reached the rollover point using Cs alone, i.e., just prior to the intentional introduction of an oxidizing agent. The activations were then finished out with both alkali sources on at a current consistent with that required to perform the single alkali activations in similar times. The only adjustment made was in the NF_3 pressure.

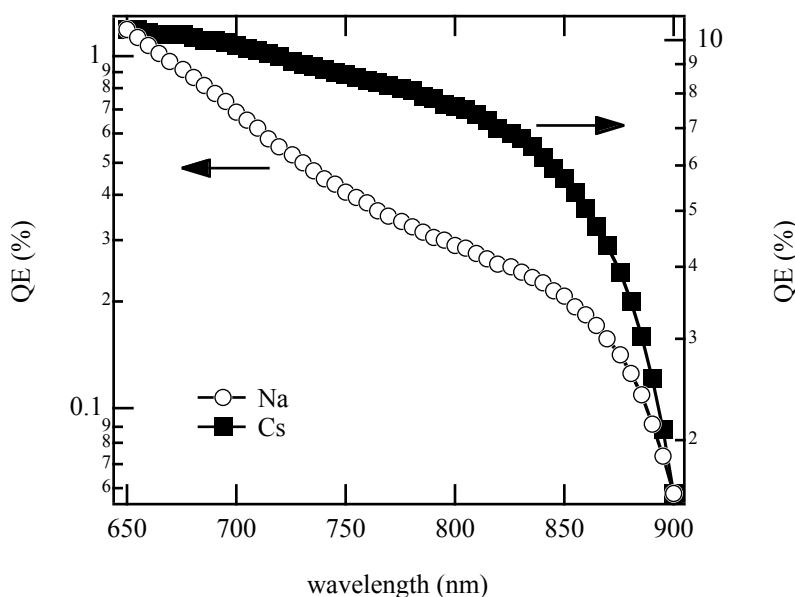


Figure 9. Quantum yield as a function of wavelength for single alkali activation of bulk GaAs using Na and Cs.

An example gas exposure illustrating the standard timeline is shown below in figure 10. Lifetime data were primarily taken with a HeNe laser, but an 850 nm thermally stabilized diode laser was used for comparison of near bandgap behavior with that far from the bandgap. The time axis is broken into three parts. The first 30 minutes corresponds to background gas exposure, the second and third to 30 minute exposures at 1.5×10^{-10} Torr CO_2 and 5.0×10^{-10} Torr CO_2 , respectively. These times and pressures were selected to provide total exposures of at least an order of magnitude higher than that expected in a typical RF gun. Typical end of CO_2 exposure cycle yield drop at 633 nm for Cs only activated samples was x15-x20.

The final-stage deposited dual alkali photoemitter yields were all lower than those with Cs alone. The normalized yield lifetimes are shown in Fig. 11. These data were not encouraging and made clear that the hypothesis of “plugging the hole” by second alkali deposition in the final activation stages was not entirely valid. However, careful study of the decay curves revealed an interesting

trend in the low CO₂ exposure data for Li and Na. Their slopes in the intermediate position were more nearly linear than those of the Cs, Rb and K activated photoemitters which exhibited faster decay rates in that region. The difference in slopes indicated that the presence of these two as second alkalis was having some effect on the decay properties of the activated photoemitters.

At this point, we had not yet determined whether there existed a combination of either Na and Cs or Li and Cs which would provide the desired immunity without deleterious effects on the final yield. As an attempt to increase the immunity, activations were attempted by co-deposition of Li and Cs during the entire process. However, the presence of Li or Na served to suppress the yield when used with Cs nearly as badly as when those alkalis were used by themselves.

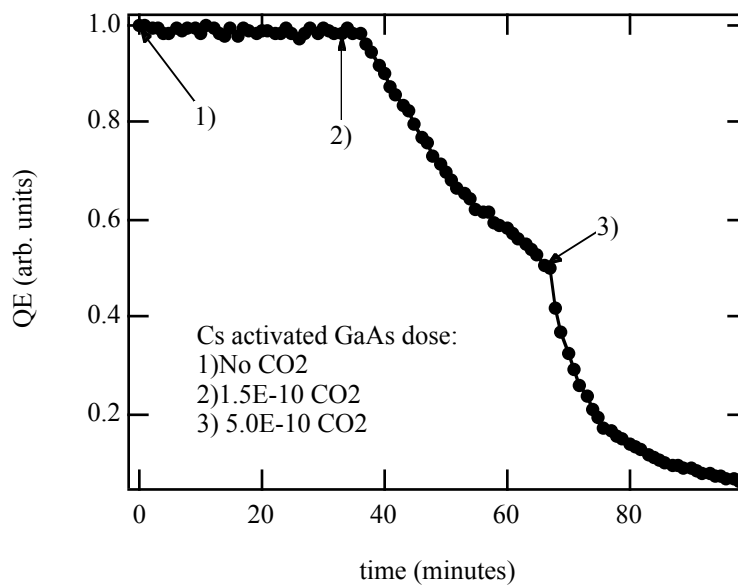


Figure 10. Normalized quantum yield decay for Cs activated photocathode using our standard exposure schedule.

A breakthrough occurred when the plan to apply the second alkali only for periods long enough that a change in yield could be observed, then repeat at a later time was formulated. We call this the “alkali spritz” technique. The activation began with both sources on at their deposition current. When the photocathode started to show real photoresponse, the second alkali deposition was ceased, later to be started anew when the first neutral density filter was inserted, when the second neutral density filter was inserted and after the oxidizer dosing has begun and lastly toward the end of the activation. An annotated activation plot is shown below in figure 12, for a Li + Cs activated photoemitter with the raw data in the form of a scanned chart in figure 13.

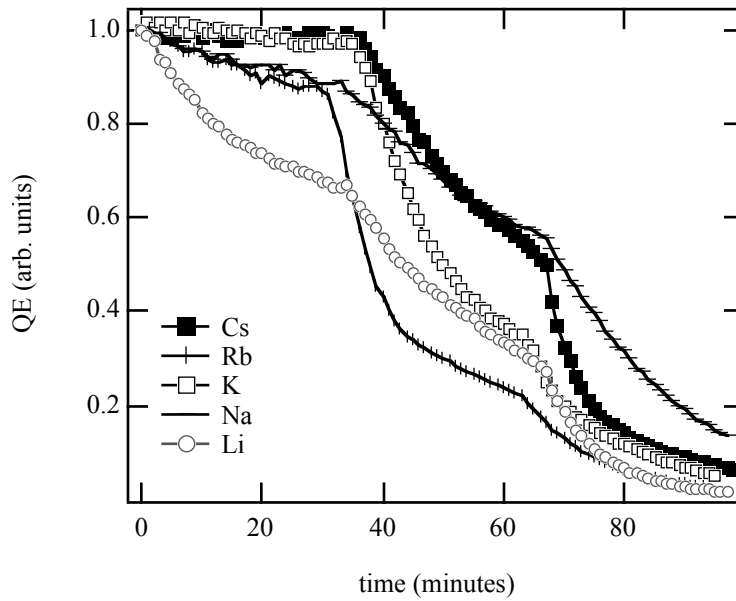


Figure 11. Normalized quantum yield decay for photocathodes activated in the usual fashion but for the addition of the indicated second alkali in the final stages of the process. The absolute yield from the photoemitters with Na and Li as the second alkali was greatly suppressed.

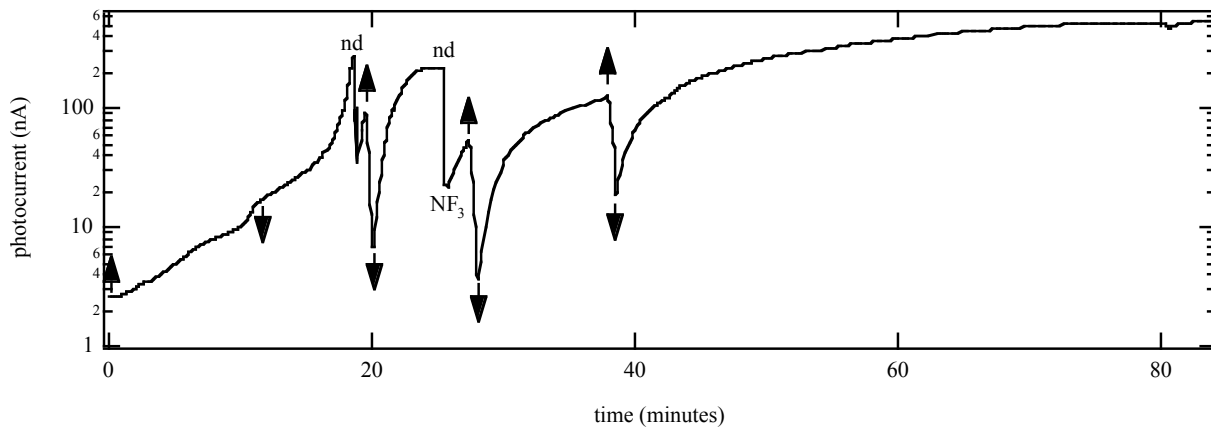


Figure 12. Activation curve from figure 13, but on a log scale and annotated for clarity. Up arrows indicate the point where the Li deposition began and the down arrows indicate the time when the Li deposition ceased. Insertion of neutral density filters is denoted by 'nd'. Oxidizer dosing is indicated by 'NF₃'.

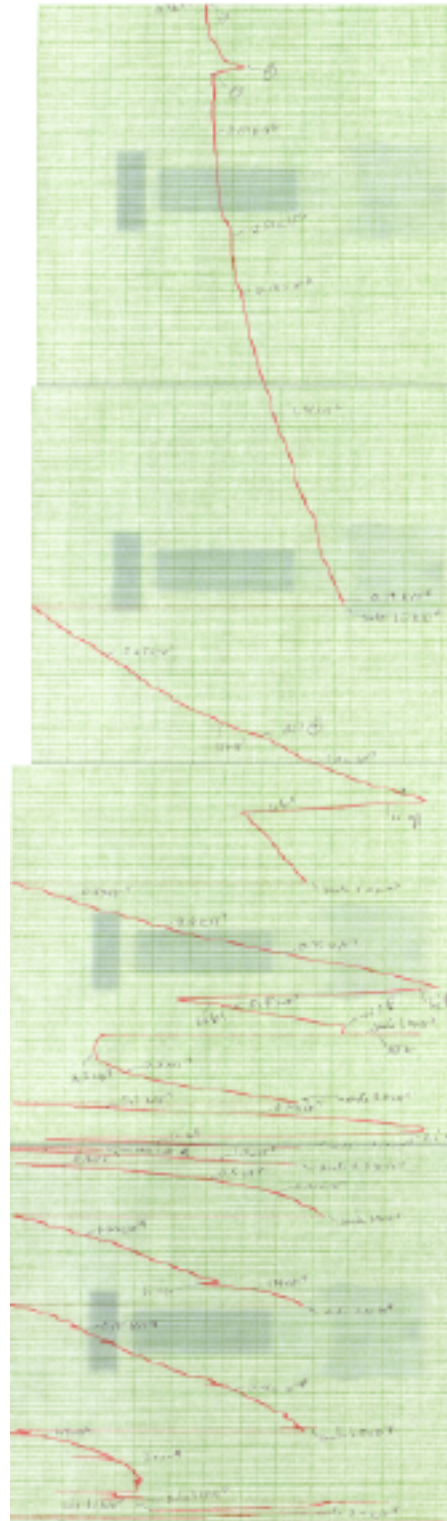


Figure 13. Scan of the activation chart recorder plot for the optimized dual Cs and Li activation of bulk GaAs. The time axis is vertical and the photocurrent axis is horizontal with increasing current toward the left.

But for the first co-deposition period, each application of the Li resulted in a drop in photocurrent of about one order of magnitude. This set the duration of each of the latter three Li exposures. In the case of Na + Cs, the application of the Na did not cause such a dramatic drop in yield, so its spritzing time was derived from those in the Li activation schedule. Highest yield was maintained by peaking up the photocathode with Cs only. Using any of the other alkalis resulted in the yield diminishing from whatever value it had before peaking was attempted.

The ordering of the spritzing was investigated as well as the effect of the total number of dosings. This was tested both for Cs + Na activations and for Cs + Li activations. For Cs + Na activations, the following was observed at the end of the standard exposure schedule:

1. Full Cs + Na spritz activation: x5.5 drop
2. Na on only at start (1 spritz): x8.9 drop
3. Na on toward end (2 spritzes): x9.1 drop

It is clear that the best immunity was obtained when the full 4 spritzes were used, though lesser improvements could be had by fewer Na dosings.

For Cs + Li activations, the following was observed at the end of the standard exposure schedule:

1. Full Cs + Li spritz activation: x6.4 drop
2. Li on from start (2 spritzes): x6.3 drop
3. Li on toward end (3 spritzes): x8.4 drop

Just as in the case of Cs + Na, the best immunity was obtained when the second alkali was on at the start of the activation. An example decay curve is shown below in figure 14. Lesser enhancement, though still an improvement over the standard activation photoemitter immunity, was obtained with the application of the Li at later times or for fewer spritzes. It is not yet clear why the two modified activation schedules result in lower reactivity, though at least two explanations are possible. In the first, Li (or Na) is tightly binding to the most active sites on the clean GaAs surface resulting in effective neutralization of those sites with respect to future reactions with background gasses. In the second explanation, the low dosage Li (or Na) arranges itself in a regular overlayer with respect to the GaAs(100) surface, thereby forcing the Cs atoms to occupy a subset of the nominal sites on the GaAs surface, effectively limiting the Cs mobility within the confining area of the Li (or Na) atoms. Limited mobility may result in fewer advantageous configurations for subsequent adsorbate reaction.

The least decay with CO₂ exposure was achieved with a Cs only activation by severely overcesiating the photoemitter. This resulted in an operationally undesirable lowering of the starting yield but did improve the peak photocurrent drop to x11 (x2 improvement). While an improvement in the drop was seen on standard activation photocathodes experiencing our exposure scheme, it was still not as good as that for photoemitters with optimal bi-alkali activations.

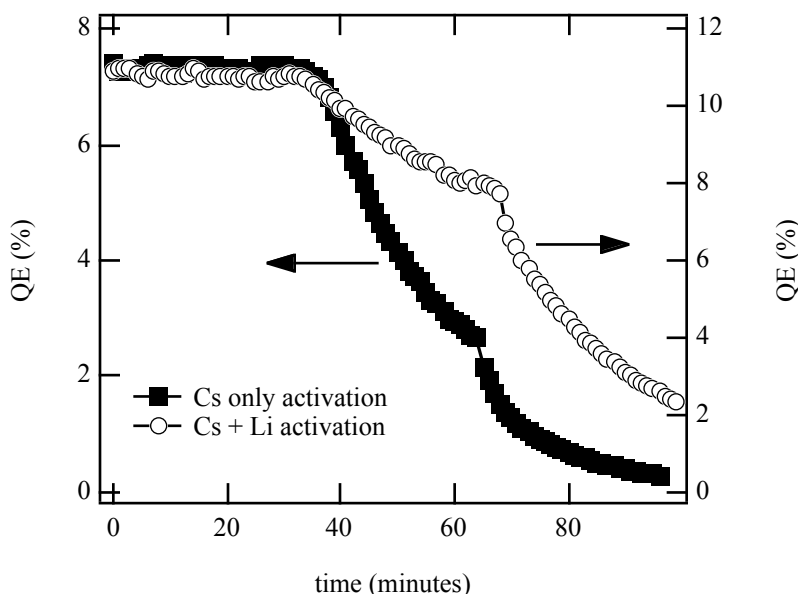


Figure 14. Comparison of yield decay at 633 nm for Cs only and Cs + Li activated bulk GaAs.

After a degree of yield immunity was achieved at 633 nm for bulk GaAs, we investigated the performance of bulk GaAs near the bandgap using an 850 nm thermally stabilized diode laser as a light source. Activation and subsequent peaking of the photocurrent was still performed with a HeNe laser. Normalized yield decay data for bulk GaAs activated with Cs only and with Cs + Li are shown below in figure 15. Comparison with the data just above in figure 14 illustrates that the near bandgap decay performance did not appreciably change for the lower pressure CO₂ exposure relative to the far from the bandgap decay behavior, though the Cs + Li activated material was still superior to the standard activation photocathode. However, for the higher pressure CO₂ exposure, the yield for both flavors of activation was not as robust as that far from the bandgap. The relative immunity of the two types of activation were vastly different. The standard photocathode dropped to only 0.15% of its original value, while the Cs + Li activated cathode dropped to 3.9% of its original value. The Cs + Li photocathode exhibited a x26 greater stability over the standard activated cathode.

While not a specified task, after investigating the near bandgap performance of bulk GaAs, tests were performed on thin, unstrained MBE grown GaAs. This material has a time response more in keeping with potential applications in RF guns though the near bandgap photoresponse is considerably lower than for bulk GaAs. In addition, the use of a different material helped us determine whether the results we had observed up to that point were or were not specific to the wafers under test. The results of the lifetime measurement at 850 nm for the 100 nm thick GaAs are shown below in figure 16. Contrary to what was expected, this material, when Cs + Li activated, actually evinced much better immunity with respect to the Cs only activated surface than the bulk material did near the bandgap. The observed difference in lifetimes at the band gap was huge. How high polarization material performs with this treatment is of much interest and will be part of the Phase II program.

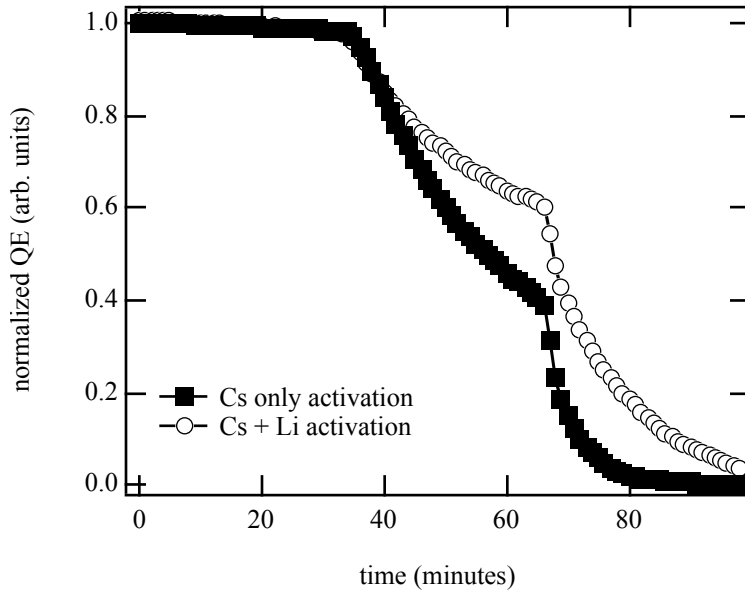


Figure 15. Normalized yield decay at 850 nm for bulk GaAs.

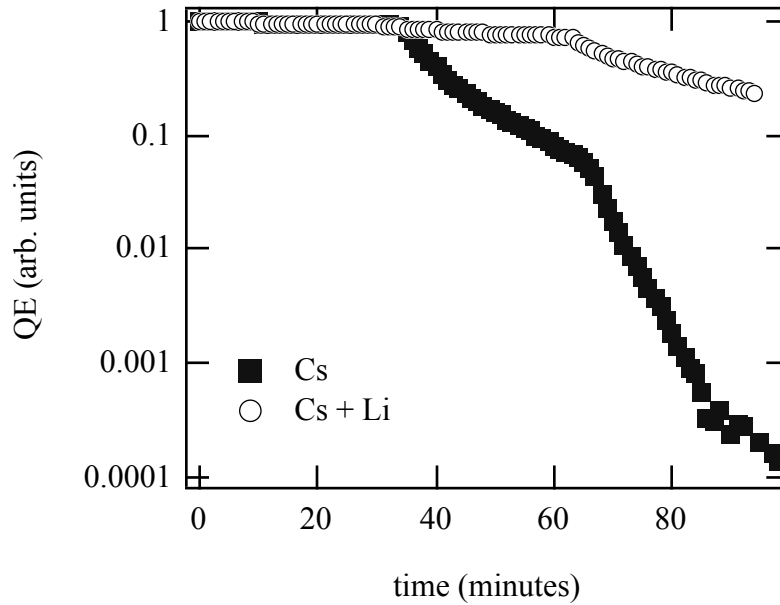


Figure 16. Normalized yield decay at 850 nm for thin, MBE grown GaAs. Note the log scale used for the QE. The starting yield of the thin material was x4 lower for the Cs + Li activated surface. However, no optimization was performed and even taking this into account, the yield decay at the end of the CO₂ exposure is still more than two orders better than for the standard activated material.

Yield data for bulk GaAs as a function of wavelength for the three different activation cases is

shown in figure 17. The optimally combined Cs + Li activated photocathode actually exhibits a yield somewhat greater than the standard sample. This effect reproduced over many samples. An interesting change in the shape of the yield curve for the Cs + Li photoemitter occurs at the bandgap. The yield curve shape at the bandgap can be dominated by the doping concentration. Higher doping results in more states transferred past the band gap edge which leads to a smearing of the band edge photoyield. For very high doping, the yield at the band gap will be diminished compared to that from lower doped material. However, the yield far from the band gap for the more highly doped material will be greater. The yield curve for the Cs + Li activated photoemitter is reminiscent of that modification. However, since the Cs and Li atoms are at the near surface, the change must represent a surface barrier modification. The Cs + Na activated material did not evince any shape change in yield when compared to the Cs only activated surface.

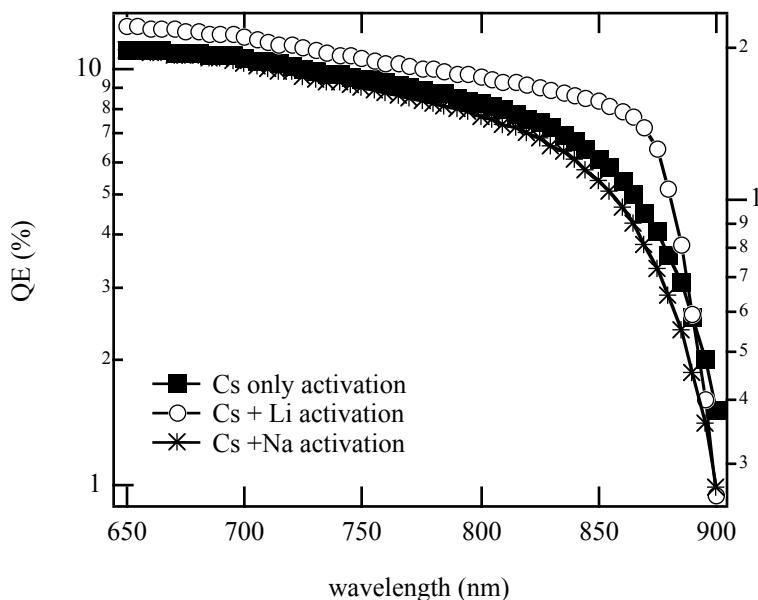


Figure 17. Quantum yield as a function of wavelength for Cs, Cs + Li and Cs + Na activated bulk GaAs.

D. Reactivity of vicinal cut GaAs

To determine how the surface quality affects the CO_2 reactivity (see e.g., the thin GaAs data in figure 16 above), two sets of miscut bulk GaAs wafers were tested for reactivity both with the standard activation method and with the optimized Cs + Li process. As may be seen below in figure 18, the presence of additional step edges on the 5° miscut material did not appreciably change its performance with respect to that of the 0.5° miscut material. In fact, the Cs + Li activated material decay curves are nearly identical despite the slightly different surface orientations. This is not to say that surface defects do not play a significant role in the surface reactivity, merely that the quantity and reactivity of the additional step edges were not sufficient to change the overall performance.

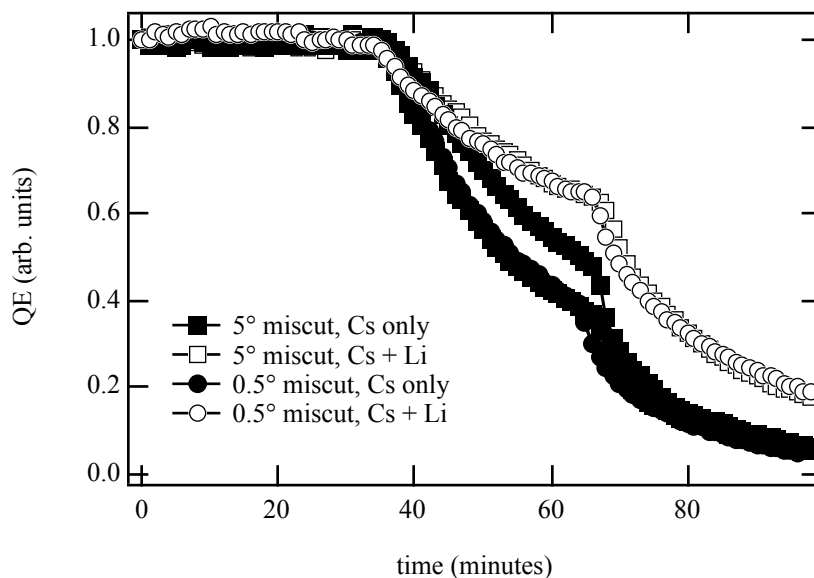


Figure 18. Normalized yield decay for 5° and 0.5° miscut GaAs.

E. SLAC measurements on composition

The sample characterization at SLAC consisted of XPS measurements on bulk GaAs photocathodes activated and immunity tested at Saxet Surface Science. The tested samples were removed and packaged in dry nitrogen filled containers and then shipped to Bob Kirby at SLAC where they were promptly installed into the load chamber of the VG small spot XPS system of the Surface and Materials Science Department. The Al K_{α} x-ray source (1486.6 eV) size at the sample was 4 mm x 4 mm. The samples were 13 mm x 13 mm squares with an exposed circular activation area of 11 mm. XPS data were acquired with the hemispherical energy analyzer set at 50 eV fixed pass energy using a 4 mm slit width resulting in a total instrumental energy resolution of 0.8 eV. The sample to analyzer entrance lens distance was 25 mm. The data were fit using a custom analysis program. Individual peak areas were corrected for photoionization cross section and the result normalized to 100%. The typical depth from which concentration information was sampled was 3-5 nm.

Within the analysis chamber, the samples were atop-, but not affixed to- an aluminum plate. For this reason, contact may not always have been electrically complete, so absolute energy values may be off by some small values. This was worked around by using either the C 1s or the O 1s peak as an energy reference. The initial pair of cathodes were submitted as blind samples, A & B (A = Cs only, B = Cs + Li). Surveys and high-resolution scans with windows around the As, Ga, Cs, F, O, C, and Li peak energies were conducted. These survey spectra are shown in figures 19 and 20.



Figure 19. XPS survey spectrum of sample A, Cs only activated GaAs. The x-ray source was Al K_{α} . The sample was activated and tested at Saxet then sent to SLAC for XPS work.

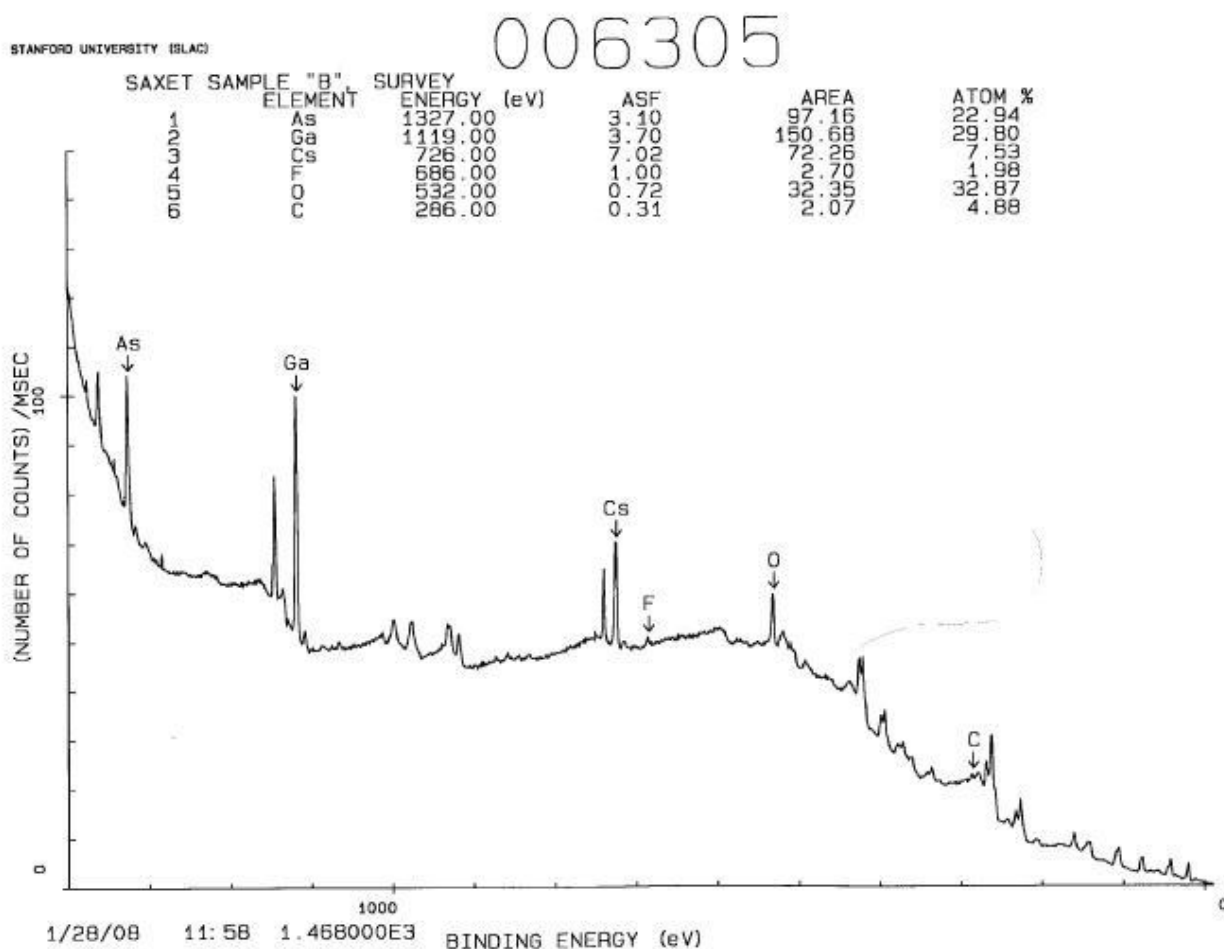


Figure 20. XPS survey spectrum of sample B, Cs + Li activated GaAs. The x-ray source was Al K_{α} . The sample was activated and tested at Saxet then sent to SLAC for XPS work.

Normalized semi-quantitative fits of the surveys (1 eV energy steps) gave, in atomic percentage:

Sample A: As-17.0, Ga-23.6, Cs-5.3, F-1.2, O-39.9, C-13.2

Sample B: As-22.9, Ga-29.8, Cs-7.5, F-2.0, O-32.9, C-4.9.

For comparison, an unactivated hydrogen-ion-cleaned bulk GaAs sample gave:

Standard: As-38.2, Ga-45.7, O-16.2, C-0.

The Ga to As composition ratio was not detected as equal to one because the outermost surface layer was an As oxide, with the oxygen shadowing the underlying As atom, hence a lowered As signal.

No lithium signal was detected on the Saxet samples. In hindsight, the reason is apparent upon examining the Li 1s (59.8 eV binding energy) photoionization cross section as a function of photon energy[1]. For the Al K_{α} energy, the Li cross section is quite small. However, the Na 1s cross section is about x100 that of the Li 1s at 1487 eV. Since the immunization results were similar for Cs + Na activated GaAs, it was decided to take data as follows: First a survey was conducted on a Na-only Saxet activated sample to insure the Na signal would be measurable. Next, a Na + Cs sample was characterized to look for differences between it and the purely-Cs activated and the purely-Na activated sample spectra. These data, as show in figures 21 and 22, provided the desired comparative compositional makeup of the Na immunized photocathode.

Na activated sample: As-15.4, Ga-20.8, Na-14.2, Cs-1.6, F-2.4, O-39.7, C-6.0
 Cs + Na activated sample: As-20.0, Ga-25.5, Na-6.0, Cs-5.4, F-3.8, O-33.6, C-5.7.

The concentration of Na and Cs was about equal on the Na + Cs activated sample even though the exposure time with the Na source on was only about 20 % of the time the Cs dispenser was emitting. However, it was on at the start of the activation, so it is likely that the majority of the Na was put down at that time (see earlier discussion on the activation process). It is interesting to note that for both the two alkali samples, the oxygen content relative to the single alkali activated samples was reduced. Of some concern is the presence of a Cs signal on the nominally Na-only activated sample. It is not clear whether this arose from cross contamination of the alkali sources in the activation process, Cs migration from the sample holder, or was due to a low partial pressure of Cs in the activation chamber.

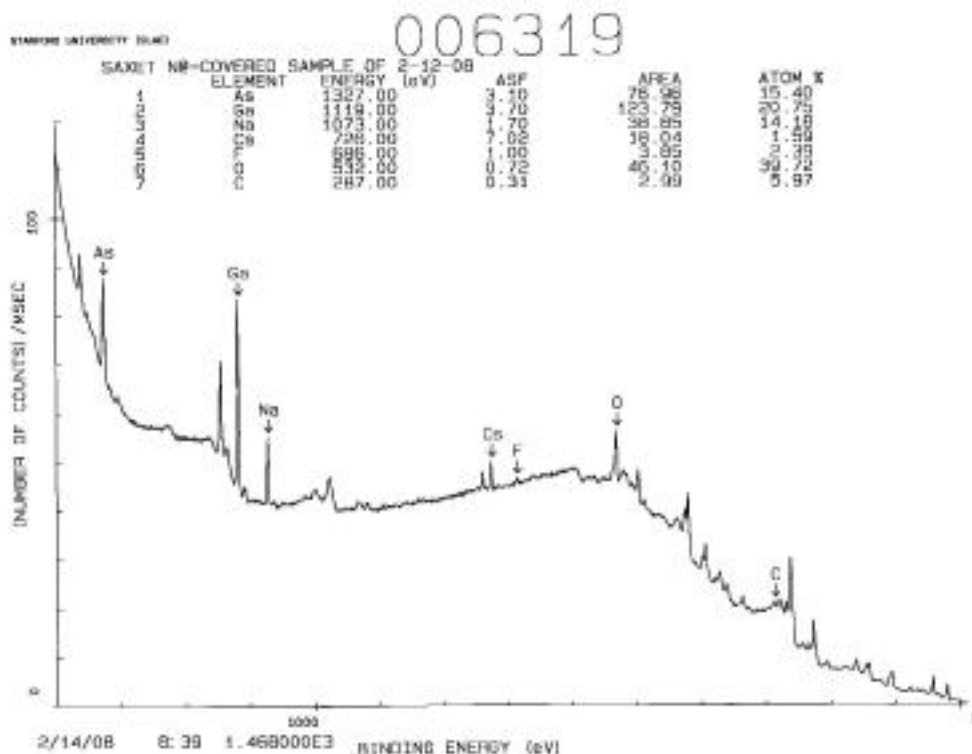


Figure 21. XPS survey spectrum of Na only activated GaAs.



Figure 22. XPS survey spectrum of Na + Cs activated GaAs.

1. J. J. Yeh and I. Lindau, Atomic Subshell Photoionization Cross Sections and Asymmetry Parameters: $1 \leq Z \leq 103$, *Atomic Data and Nuclear Data Tables* **32**, 1 (1985).